Adsorption of Methyl Orange on Bentonite: Design, Modeling, and Analysis of Experiments

Bessaha, Fatiha*[*+]*; Bessaha, Gania; Ziane, Samira; Khelifa, Amine

Laboratory of Structure, Elaboration and Applications of Molecular Materials (S.E.A.2M.), Department of Process Engineering, Faculty of Science and Technology, University of Mostaganem, B.P. 981, R.P., Mostaganem 27000, ALGERIA

ABSTRACT: *The study examines the possibility of removing Methyl Orange (MO) from aqueous solutions using crude bentonite. SEM-EDX (scanning electron microscopy) and XRD (X-Ray Diffraction) analyses were performed to characterize the material. Batch experiments were performed on the adsorption process to study the effect of contact time, pH, concentration, and temperature. The results indicate that the equilibrium reaches after 2 h of contact. The MO adsorption followed the Langmuir-Freundlich and Baudu models with a maximum adsorption capacity of 308 mg/g. The adsorbed capacity of the material is best at pH=3. The adsorption capacity increases with temperature. In addition, the Central Composite Design (CCD) in Response Surface Methodology (RSM) and Artificial Neural Network (ANN) were used to evaluate the simultaneous interactions of independent variables. The results suggest that the initial concentration was the dominant parameter in the adsorption process. The monolayer model with two energies derived from statistical physics can be adapted to interpret the adsorption data. Physical adsorption forces were predicted to be responsible for the removal of the dye. This study provides new information on the adsorption mechanisms of pollutants commonly found in water.*

KEYWORDS: *Methyl orange; Modeling, Raw bentonite; Statistical physic.*

INTRODUCTION

Currently, water pollution is a global problem that affects human health and leads to environmental pollution. This water is contaminated by several pollutants such as heavy metals, dyes, and antibiotics. These pollutants are very toxic and cause irritation to the respiratory and gastrointestinal tracts of humans [1]. In addition, they are initiators that can cause cancer and severe eye irritation in humans [2]. MO is a dye poorly biodegradable and its presence in the aquatic environment affects the life span and reproductive capacity of aquatic organisms by decreasing photosynthetic activity and minimizing sunlight penetration [3]. Adsorption, coagulation, ozonation, oxidation, and photodegradation are methods used to treat colored effluents [4,5]. Some processes are very effective, although they require the use of concentrated chemicals that accumulate biologically or involve expensive environmental remediation equipment. Adsorption technology remains the most favorable approach to large-

**To whom correspondence should be addressed.*
+ E-mail: fatiha_bessaha@yahoo.fr
1021-9986/2023/10/3306-3323 18/$/6.08

scale wastewater treatment [6 ,7]. Therefore, it is necessary to continue research for developing eco-friendly and low-cost adsorbents. For the removal of MO from water unconventional adsorbents have been reported in the literature for their capacity, such as cellulose nano-crystals [8], nanocomposite (CS–AgNC) [9], biochar [10], Perlite [11], and NaX/MgO–TiO_2 Zeolite [12]. Activated carbon is the most widely used adsorbent for industrial applications [13], but it is expensive for each adsorption cycle. Therefore, it is important to identify less expensive, more efficient, and more locally available materials to decolorize wastewater. Clays have been identified as an interesting and promising class of adsorbent materials for this application [14,15]. Bentonite is a clay mineral, which is mainly consisting of montmorillonite. It is a 2:1 aluminosilicate, whose unit layer structure consists of an octahedral $A1^{3+}$ sheet placed between two tetrahedral Si^{4+} sheets. In addition to these favorable adsorption properties, regeneration of these cheap and abundant resources is not necessary, whereas it is crucial for conventional adsorbents.

RSM and ANN are among the most popular methods capable of predicting process efficiency with acceptable error. RSM is widely used for the design and optimization of experimental data [16]. It is a powerful tool to determine the best operating conditions for the desired response with less experimental data, providing a mathematical model for the response based on the analyses performed [17].

On the other hand, ANNs are considered universal approaches, due to their strong generalization power. ANNs have no limit in the correlation of non-linearities. Inspired the functioning of the human brain, the neural network uses artificial neurons connected in parallel layers [18]. Among the existing ANN models, the multilayer perceptron is the most used because it allows the modeling of highly nonlinear processes through different layers of neural networks. To optimize the input parameters from their fit, it is necessary to couple the ANN with a global search algorithm to perform this function [19].

The objective of our work is to use raw bentonite for the adsorption of an acid dye MO. The study consists in evaluating the effect of pH, contact time, concentration, and temperature. We examine the modeling of the adsorption isotherms by two, three, and four-parameter models. The determination of statistical errors was also examined. Optimization of the adsorption parameters has been performed by two models RSM and ANN. Particular attention was given to determining the adsorption mechanism by statistical physics theory.

EXPERIMENTAL SECTION

Material

The bentonite utilized is from a source located in western Algeria (Mostaganem). X-ray powder diffraction was collected utilizing a RIGAKU diffractometer of CuKa radiation running at 40 kV and 25 mA. Range of 5-80° with a rate of 0.01° are the conditions of XRD. A JEOL, JSM-6360 was used to determine the chemical composition of raw bentonite *via* energy dispersive X-ray spectroscopy (EDX) analysis attached to SEM.

Methods

Adsorption experiment

800 mg of MO (chemical formula $C_{14}H_{14}N_3NaO_3S$; λ_{max}= 466 nm, obtained from biochem Chemopharma) was dissolved in 1 L of water. 20 mL of MO solution mixed with 20 mg of raw bentonite. The pH varies from 3 to 9, contact time (3- 240 min), initial concentration from 100 to 600 ppm, and temperature from 25 to 55 °C. We mixed the suspension at 180 rpm (Julabo SW22, Germany). At equilibrium, centrifugation separates the solution at 4000 rpm for 40 min. The Shimadzu 1240 UV-Vis spectrophotometer measure the absorbance at 466 nm. The equation determines the adsorbed amount is:

$$Q_e = \frac{(C_0 - C_e) \times V}{m} \quad (1)$$

Where

C_e : Equilibrium concentration (mg/L)

C_0: Initial dye concentration (mg/L)

V: Adsorbat volume (L)

m: Sorbent mass (g)

THEORETICAL SECTION

It is necessary to evaluate and optimize the design of an equilibrium adsorption model. The characteristics of the adsorbent properties, sorption system, and complexation interactions at the solid-liquid interface are all significant information given by the adsorption isotherm. In this study, Eight nonlinear models with 2, 3, and 4 parameters were employed to model the data isotherms, and three models for kinetic study.

Kinetic models

pseudo-first-order

$$Q_t = Q_e\ (1 - e^{-k_1 t}) \quad (2)$$

pseudo-second-order

$$Q_t = \frac{k_2\ Q_e{}^2\ t}{1+k_2\ Q_e t} \quad (3)$$

Intraparticle diffusion

$$Q_t = k_{id}\ \sqrt{t} + l \quad (4)$$

Q_t : Adsorption amount at time t (mg/g) ;
k_1: pseudo-first-order rate constant (min^{-1}) ;
t:: Contact time (min)

$$h = k_2\ .\ Q_e^2 \quad (5)$$

h: Initial adsorption rate
k_{id} : Intraparticle diffusion rate constant (mg/(g.$min^{1/2}$))
l : Constant

Isotherm models

Langmuir

$$Q_e = \frac{q_{mL}\ K_L\ C_e}{1+K_L\ C_e} \quad (6)$$

q_{mL} : Amount required to fill a monolayer(mg/g);
K_L: Langmuir constant related to the energy of adsorption (L/mg)

Freundlich

$$Q_e = K_F\ C_e^{\frac{1}{n}} \quad (7)$$

$\frac{1}{n}$: Parameter in relation to adsorption intensity
K_F: The Freundlich equilibrium isotherms constant (L/g)

Temkin

$$Q_e = \frac{RT\ ln\ (K_T\ C_e)}{b} \quad (8)$$

R: The universal gas constant, R = $8.314\ J/mol\ K$; T: Temperature (K) ; K_T: The Temkin
K_T: The Temkin equilibrium isotherms constant (L/g)
b: The Temkin constant which is related to the heat of sorption (J/mol)

Redlich-Peterson (R-P)

$$Q_e = \frac{K_{RP}\ C_e}{1+\left(a_{RP}\ C_e^{\beta}\right)} \quad (9)$$

a_{RP} : Constant (L/g); β: Heterogeneity factor depending on the surface properties of the material
K_{RP}: The Redlich-Peterson equilibrium isotherms constant (L/g)

Langmuir- Freundlich (L-F)

$$Q_e = \frac{q_{mL-F}\ (K_{L-F}\ C_e)^{m_{L-F}}}{1+(K_{L-F}\ C_e)^{m_{L-F}}} \quad (10)$$

q_{mL-F} : The Langmuir--Freundlich maximum adsorption capacity (mg/g) ;
K_{L-F}: The equilibrium constant for a heterogeneous

Toth

$$\mathrm{Q_e} = \frac{q_{mT}\ C_e}{\left(\frac{1}{K_T} + C_e{}^{m_T}\right)^{\frac{1}{m_T}}} \quad (11)$$

q_{mT} : The Toth maximum adsorption capacity (mg/g) ; K_T: The Toth equilibrium isotherms constant (L/g) ; m_T: the Toth model exponent

Khan

$$\mathrm{Q_e} = \frac{q_{mK}\ b_K\ C_e}{(1+b_K\ C_e)^{\beta}} \quad (12)$$

q_{mK} : The Khan maximum adsorption capacity (mg/g) ; b_K : The Khan isotherm equilibrium constant; β: The Khan model exponent

Baudu

$$\mathrm{Q_e} = \frac{q_{m0}\ b_0\ C_e{}^{(1+x+y)}}{1+b_0\ C_e{}^{(1+x)}} \quad (13)$$

y: The Baudu isotherm parameter
q_{m0} : The Baudu maximum adsorption capacity (mg/g) ;
b_0: The Baudu isotherm equilibrium constant ;
x: The Baudu isotherm parameter

Errors equations

To evaluate the adequacy of the data prediction of isotherm and kinetic models, error function models were applied.

Coefficient of determination (R^2)

$$\mathrm{R^2} = 1 - \sum_{i=1}^{N} \frac{\left(y_{cal} - y_{exp}\right)^2}{\left(\bar{y}_{exp} - y_{exp}\right)^2} \quad (14)$$

Adjusted coefficient of determination (R^2_{adj})

$$R^2_{adj} = \sum_{i=1}^{N} \frac{(Q_{exp} - Q_{cal})^2}{Q_{cal}} \quad (15)$$

Residual Root Mean Square Error (RMSE)

$$RMSE = \sqrt{\frac{\sum_{i=1}^{N} (Q_{exp} - Q_{cal})^2}{N}} \quad (16)$$

Sm of the Squares of the Errors (SSE)

$$SSE=\sum_{i=1}^{N}(Q_{exp}-Q_{cal})^2 \quad (17)$$

« exp » and « cal »: The experimental and calculated values; N : the number of observations in the experimental data ; P: The number of parameters in the model.

Response surface methodology

The RSM uses mathematical and statistical modeling tools to approximate and optimize the key parameters that influence the behavior of a particular response. This model was employed to find the optimal combination of experimental data obtained from the preliminary tests one factor at a time using the Central Composite Design (CCD). It can take into account a variety of factors and provide accurate predictions. In this work, time, starting concentration, pH, and temperature are four independent variables utilized to fit the CCD using the second-order polynomial quadratic equation (18), while the removal capacity of the raw bentonite is the response variable. Analysis of variance (ANOVA) statistics is employed to determine the accuracy and significance of the fitted model. The model with the highest F-value and lowest P-value at a 95% confidence level indicated a better arrangement of the input parameters [20].

$$y=\beta_0+\sum_{i=1}^{k}\beta_i x_i+\sum_{i=1}^{k}\beta_i x_{ii}^2+\sum_{i<j}^{k}\beta_{ij}x_i x_j \quad (18)$$

Where k: factors number, xi, and xj are independent variables, y is the appropriate response, i: Linear coefficient, and ij: Interaction coefficient, β_0: Constant, β_i: linear coefficient, $\beta_{ij\ is}$: Interactive coefficient.

Artificial neural network

ANN consisting of an interconnected group of artificial neurons is a mathematical model or computational model. In most cases, an ANN is an adaptive system with the ability to learn from existing data and adapt to match a set of input parameters to a set of output parameters, without knowing the complex relationship between them, and to change its structure according to external or internal factors. Different back-Propagation (BP) algorithms were evaluated to select the most appropriate back-propagation algorithm. The Marquardt-Levenberg learning algorithm with minimum Means Square Error (MSE) is the best. The ANN model and the variation of its parameters were determined according to the minimum value of the MSE of the set of and prediction set.

Physical models MO analysis

To interpret the adsorption of the pollutant onto the adsorbent, four physical models are performed.

Monolayer adsorption model

$$Q_e=\frac{nD}{1+\left(\frac{C_{1/2}}{C_e}\right)^n} \quad (19)$$

n: The bonded number of dye molecules (MV) by the adsorbent functional group; $C_{1/2}$: The concentration at half-saturation ; D: density of functional groups assuming that the functional groups can be occupied by the dye molecules at saturation.

Monolayer adsorption model with two energies

$$Q_e=\frac{n_1 D_{1m}}{1+\left(\frac{C_1}{C_e}\right)^{n_1}}+\frac{n_2 D_{2m}}{1+\left(\frac{C_2}{C_e}\right)^{n_2}} \quad (20)$$

n_1 and n_2 represent the number of captured MV molecules per leading site of the first and of the second type, respectively; D_{1m} and D_{2m} represent two types of densities of receptor sites; C_1 and C_2 are the half-saturation concentrations of the first and second site type, respectively

Double-layer adsorption model

$$Q_e=nD\frac{\left(\frac{C_e}{C_1}\right)^n+2\left(\frac{C_e}{C_2}\right)^{2n}}{1+\left(\frac{C_e}{C_1}\right)^n+\left(\frac{C_e}{C_2}\right)^{2n}} \quad (21)$$

C_1 and C_2 are the concentrations at half-saturation related to the first and second layers, respectively.

Multi-layer adsorption model

These models have several assumptions. The model is expressed by the variation of the adsorbed amount as a function of the concentration.

In the first model (physical monolayer model), the MO dye molecules were predicted to bind in a single layer on the adsorbent surface of the raw bentonite, with each molecule having single adsorption energy.

The second model (physical monolayer model with two energies), in contrast to the assumptions of the first model, considered that the adsorption of MO on the bentonite could appear on two distinct classes of receptor sites, each with a different energy. This indicates that the MO dye adsorption in this case was caused by two different types of receptor sites present in the bentonite adsorbent.

$$Q_e = nD \frac{\frac{-2\left(\frac{C_e}{C_1}\right)^{2n}}{1-\left(\frac{C_e}{C_1}\right)^{n}} + \frac{\left(\frac{C_e}{C_1}\right)^{n}\left(1-\left(\frac{C_e}{C_1}\right)^{2n}\right)}{\left(1-\left(\frac{C_e}{C_1}\right)^{n}\right)^{2}} + \frac{2\left(\frac{C_e}{C_1}\right)^{n}\left(\frac{C_e}{C_2}\right)^{n}\left(1-\left(\frac{C_e}{C_2}\right)^{nN_2}\right)}{1-\left(\frac{C_e}{C_2}\right)^{n}} + \frac{N_2\left(\frac{C_e}{C_1}\right)^{n}\left(\frac{C_e}{C_2}\right)^{n}\left(\frac{C_e}{C_2}\right)^{nN_2}}{1-\left(\frac{C_e}{C_2}\right)^{n}} + \frac{\left(\frac{C_e}{C_1}\right)^{n}\left(\frac{C_e}{C_2}\right)^{2n}\left(1-\left(\frac{C_e}{C_2}\right)^{nN_2}\right)}{\left(1-\left(\frac{C_e}{C_2}\right)^{n}\right)^{2}}}{\frac{1-\left(\frac{C_e}{C_1}\right)^{2n}}{1-\left(\frac{C_e}{C_1}\right)^{n}} + \frac{\left(\frac{C_e}{C_1}\right)^{n}\left(\frac{C_e}{C_2}\right)^{n}\left(1-\left(\frac{C_e}{C_2}\right)^{nN_2}\right)}{1-\left(\frac{C_e}{C_2}\right)^{n}}} \quad (22)$$

C_1 and C_2 are the concentrations at half-saturation related to the first and the $1+N_2$ layers, respectively.

Table 1: Chemical composition of raw bentonite

Oxide	SiO_2	Al_2O_3	CaO	Fe_2O_3	MgO	Na_2O	TiO_2	SO_3	P_2O_5
%	64.2	11.6	9.3	4.8	3.4	3.3	1.1	0.5	0.03

The third concept, called the dual-layer physical model with two energies, assumes that the development of two layers with distinct energies determines how the MO dye is adsorbed. The MO molecules interactions and the adsorbent surface were controlled by the first energy, while those between MO dye molecules in the two layers were controlled by the second energy.

Finally, the multilayer physical model was designed as a general example where the MO dye molecules were assumed to be able to bind via a variable number of layers created with two energies. The interactions of the first layer and other additional layers were responsible for the two adsorption energies, as in the previous model. Take into consideration that this model defines the total layer produced as $1 + N_2$ in its assumptions.

RESULTS AND DISCUSSION

Characterization of raw bentonite

Chemical composition of raw bentonite

Table 1 gives the raw bentonite composition. The main oxides in the material are lime, alumina, and silica. Theoretically, silica and alumina constitute 92% of the total composition of montmorillonite in its ideal structure. The ratio of silica to alumina is 2.6 [21]. The amount of silica and alumina overall in the raw bentonite utilized in this paper was 75.84 %, and the silica-alumina ratio was 5.53. This ratio was about double times the expected value, revealing that the bentonite in its natural form included a sizable amount of silica.

XRD analysis

Bentonite XRD diffractogram (Fig. 1) showed reflections of the characteristic of montmorillonite clay.

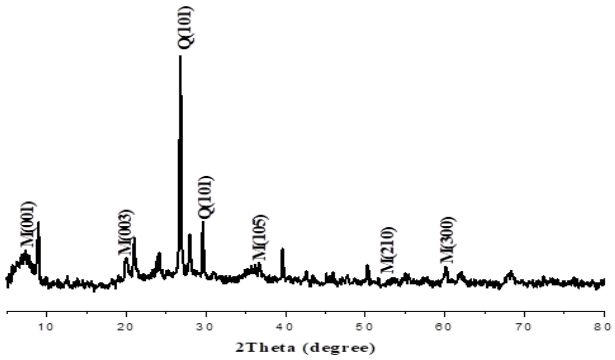

Fig. 1: X-ray diffraction of the raw bentonite

Additionally, the mineral small opal ($SiO_2.nH_2O$) and quartz (SiO_2) impurities were identified. The basal spacing value (d_{001}) was 11.77 Å, according to the base reflection observed at 7.19° (2θ). This amount was more by the classification of natural calcium bentonites [22].

SEM analysis

The morphology of raw bentonite particles was observed in the images captured using a scanning electron microscope. The particles, shown in Fig. 2, were created by heterogeneous aggregates of various sizes and shapes. These grains appear to be a stack of sheets, which probably represents the clay layers. A little, brilliant crystallite settles on the sample's surface, it may be made of free silica (quartz).

Methyl orange adsorption

pH effect

Fig. 3 gives the variation of adsorbed quantity as a function of pH. The plot indicates that quantity decreases with the increase in pH. As an example, the amount passes from 134 to 93 mg/g, for pH 3 and 9 respectively. The zero point charge (ZPC) of the material is at pH =7. The material is negatively charged at a pH below 7, and positively at a pH above 7. The maximum adsorbed quantity is best at pH=3. In the acidic medium, the tertiary amine groups of MO (pKa = 3.46)

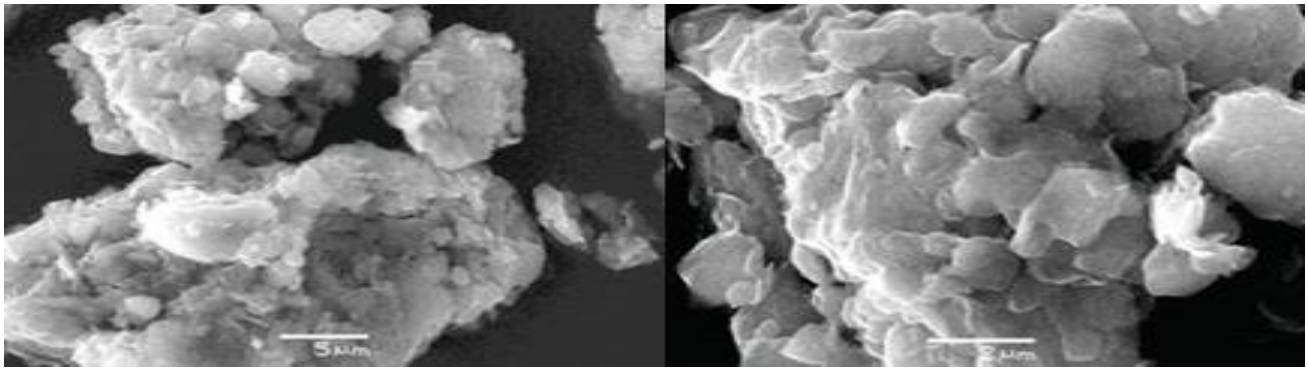

Fig. 2: SEM images of raw bentonite

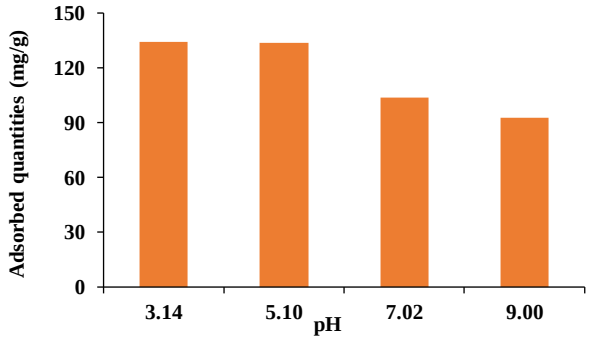

Fig. 3: pH effect on adsorption capacity of MO

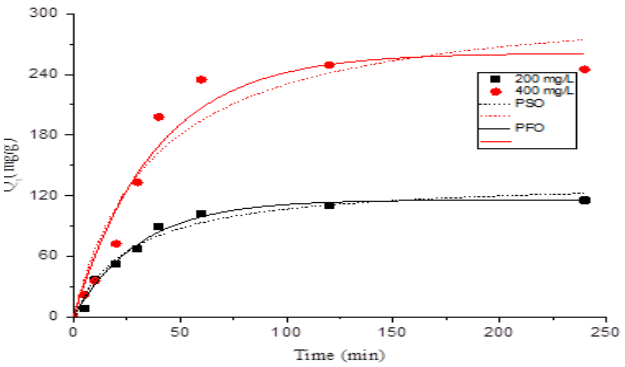

Fig. 4: Adsorption kinetic of MO on raw bentonite: data, PFO and PSO, (C=200 mg/L and C=400 mg/L)

protonates with positive charges. The interactions formed between the protonated amine and the sulfate groups of MO dye further increase the adsorption capacity [23]. *Mohammed et al*. [24] found that pH=2 is better for MO adsorption by modified zeolite.

Effect of contact time

Fig. 4 shows the adsorbed quantity variation of bentonite as a function of the contact time. The adsorbed quantity increases with the contact time. The kinetics is very fast the first time and the equilibrium reach after 2 hours. This stabilization is caused by the occupation of the active sites by the molecules. Zahrah Alhalili [25] found a time of 2 h on the removal of OM by a copper oxide nanoparticle CuO.

Effect of concentration and temperature

Fig. 5 gives the variation of MO adsorbed quantities on raw bentonite. The adsorption isotherms are L-type according to the classification of *Gile et al*.[26]. The variation of the adsorbed amount increases with temperatures. The adsorption capacity is higher at a temperature of 55 °C. The results show that the retention of MO on the bentonite surface is endothermic. As an example, the adsorption capacity is 308 mg/g at 55 °C and 159 mg/g at 25 °C.

Modeling

Using the linear method to determine model parameters is becoming a routine method. Research is moving towards the non-linear method. This method is more efficient and accurate. In addition, the use of two-parameter models in nonlinear modeling is not sufficient. Consequently, researchers develop models with three and four parameters.

To explain the kinetics of adsorption several models are available. Pseudo first order, Pseudo second order, and intraparticle diffusion. Results of modeling (Table 2) show that the PFO model applies better than PSO with an $R^2 \geq 0.97$. Whatever concentration the model applied is the same. The coincidence of experimental and theoretical quantities confirms the validity of the PSO model (Fig. 4). *Rimzim Jasrotia et al.* [27] show that the Pseudo second-order kinetic model fitted better brilliant green dye into CTAB modified ferrite composite, which indicated that the adsorption was chemical.

Table 2: Statistical metrics using non-linear (NL) approaches to evaluate the optimal parameters of the kinetic model

	Models	Pseudo first Order		Pseudo second order		intraparticular diffusion	
Metrics	Concentration	200	400	200	400	200	400
	Parameters	q_{ecal}=115.85 k_1=0.032 R^2=0.988	q_{cal}=261.13 k_1=0.0261 R^2=0.955	q_{cal}=136.41 h=4.925 k_2=2.65.10^{-4} R^2=0.974	q_{cal}=318.17 h=55.13 k_2=8.22.10^{-5} R^2=0.924	K_{id}=27.70 l=0 R^2=0.706	K_{id}=67.52 l=0 R^2=0.995
RMSE		4.987	23.16	7.48	30.08	2.29	9.98
$\chi 2$		24.873	536.59	55.97	905.27	0.16	2.33
RSS		174.114	3756.16	391.80	6336.91	26.14	497.96

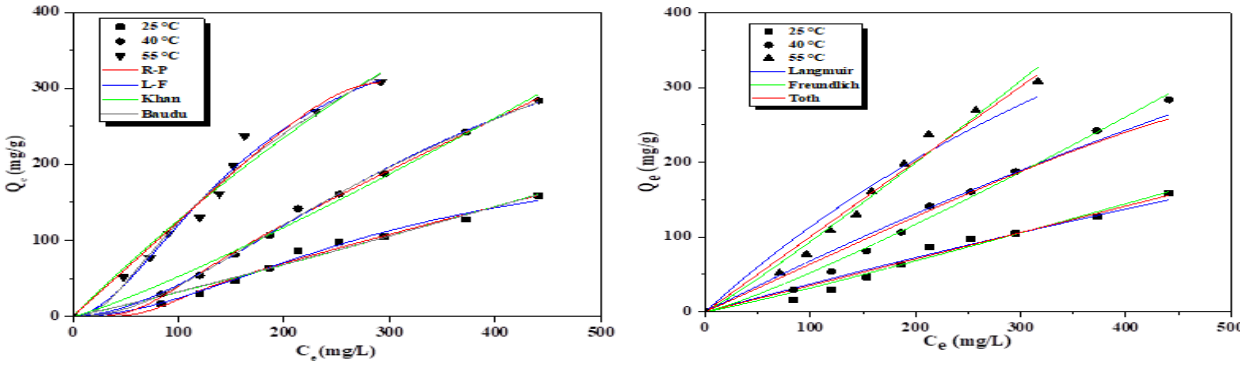

Fig. 5: Experimental and predicted isotherms of dye according to different models, at 25, 40, and 55 °C

To further confirm the adequacy of the model we used statistical errors: RMSE, $\chi 2$, and SSE. The errors of the PFO model are the lowest, with RMSE values not exceeding 23. For intraparticle diffusion Table 2 groups the calculated parameters. The values of l (l=0) show that the internal transfer is the limiting step. In addition, the external diffusion does not contribute to the adsorption kinetics.

In our study, we use Eight models to describe the adsorption isotherms (Fig. 5). The parameters of the non-linear fit of different models Fig. in Table 3.

Statistically, a two-parameter model requires less data points than the three-parameter model and the three-parameter model requires less data points than the four-parameter model. Typically, if the number of model parameters increases, the fit error reduces because a better fit can be attained and, at the same time, the overall generalization error should rise due to the higher variability of the model. It should be observed, however, that smaller models may tend to perform better for the same data set. Thus, when models with different parameters fit on the same set of data points, regardless of the assumptions of the models, the model that has a sufficient number of excess data points will provide the best fit to those data points.

The Langmuir-Freundlich and Baudu models describe the MO adsorption isotherms very well. Coefficients of determination (R^2) are greater than 0.980. In addition, errors (χ^2, RMSE) are very low compared to the other models.

The Langmuir-Freundlich model adequacy indicates the adsorption system's heterogeneity. For Baudu's model, when the parameters increase error decreases and precision increases. The results found confirmed this supposition.

For model validation, we use the information criterion test (AIC) as a new criterion. For Langmuir-Freundlich and Baudu AIC is the lowest compared to the other models. For example, for Langmuir and Langmuir-Freundlich the values of AIC at 40 °C, are 72.224 and 42.547 respectively. From the AIC values, the most suitable model is L-F for 25 °C and 40 °C, and Baudu for 55 °C. Onu et al. [28] have the same evolution in the adsorption of Eriochrome black-T by modified clay.

Comparison with other materials

Table 4 compares the MO amount sorbed by raw bentonite with other sorbents. The adsorption amount of our adsorbent is superior to the other adsorbents such as nanocomposite, chitosan, and LDH. Raw bentonite is very effective in wastewater treatment, once implemented on a large scale.

Table 3: Modeling and statistical parameters MO adsorption into raw bentonite

B	Toth			Khan			Baudu			
T=25 °C										
Parameters	q_{mt}(mg/g)	K_T	m_T	q_{mk} (mg/g)	b_K	β	q_{mb}(mg/g)	b	x	y
Errors ↓	678.767	2.8×10^{-6}	1.698	215.562	6.567×10^{-4}	0.576	299.08112	7.179×10^{-4}	-1.045	1.132
R^2	0.971			0.973			0.977			
χ^2	85.126			78.406			77.722			
SSE	681.010			627.249			544.055			
RMSE	9.226			8.854			8.816			
AIC	52.209			51.388			55.965			
T=40 °C										
Parameters	q_{mT}	K_T	m_T	q_{mK}	b_K	β	q_{mB}	b	x	y
Errors ↓	598.618	6×10^{-5}	1.513	538.745	0.054	3×10^{-7}	485.977	7.968×10^{-6}	1.139	-0.081
R^2	0.921			0.958			0.997			
χ^2	757.233			401.131			37.047			
SSE	6057.868			3209.050			259.332			
RMSE	27.517			20.028			6.086			
AIC	74.065			67.711			48.555			
T=55 °C										
Parameters	q_{mT}	K_T	m_T	q_{mK}	b_K	β	q_{mB}	b	x	y
Errors ↓	725.823	1.631×10^{-5}	1.740	580.017	0.002	0.421	723.513	7.055×10^{-5}	0.833	-0.086
R2	0.969			0.966			0.981			
χ^2	344.937			381.091			246.974			
SSE	2759.503			3048.729			1728.818			
RMSE	18.572			19.521			15.715			
AIC	66.202			67.199			67.526			

Models	Langmuir		Freundlich		Temkin		Langmuir-Freundlich (L-F)			Redlich-Peterson (R-P)		
T=25 °C												
Parameters →	q_{mL} (mg/g)	K_L (L/mg)	K_F	1/n	K (L/g)	B (J/mol)	q_{mL-F} (mg/g)	K_{L-F}	m_{L-F}	K_{RP}	a_{RP}	β
Errors ↓	638.745	6.674×10^{-4}	0.214	1.087	0.012	28.949	221.929	0.003	1.947	0.354	5.5×10^{-4}	0.005
R^2	0.953		0.969		0.976			0.988		0.973		
χ^2	121.469		77.722		69.909		38.422			78.392		
SSE	1093.225		544.056		559.269		268.957			627.139		
RMSE	11.021		8.816		8.361		6.198			8,853		
AIC	52.657		47.716		50.240		48.919			51.386		
T=40 °C												
Parameters →	q_{mL}	b	K_F	1/n	K	b	q_{mL-F}	K_{L-F}	m_{L-F}	K_{RP}	a_{RP}	β
Errors ↓	731.019	0.001	0.211	1.259	0.014	14.868	427.863	0.004	2.131	0.941	0.057	0.087
R^2	0.899		0.980		0.973		0.997			0.957		
χ^2	859.494		167.440		262.865		32.391			366.137		
SSE	7735.448		1172.086		2102.921		259.128			3295.239		
RMSE	29.317		12.939		16.213		5.691			19.134		
AIC	72.224		54.624		63.485		42.547			63.691		
T=55 °C												
Parameters →	q_{mL}	b_L	K_F	1/n	K	b	q_{mL-F}	K_{L-F}	m_{L-F}	K_{RP}	a_{RP}	β
Errors ↓	805.399	0.002	1.937	0.903	0.024	16.221	442.970	0.006	1.794	1.808	0.116	0.293
R^2	0.949		0.946		0.959		0.981			0.963		
χ^2	507.754		481.076		454.151		251.094			410.218		
SSE	4569.787		3367.534		3633.213		1757.658			3281.748		
RMSE	22.533		21.933		21.310		15.845			20.253		
AIC	66.960		64.122		68.953		67.691			67.935		

Table 4: Comparison of adsorbed quantity with other materials

Adsorbent	qe (mg/g)	References
Mesoporous material	102.40	[29]
Acid modified carbon	147.06	[30]
Carbon nanotube composite fibers	14.13	[31]
agricultural waste	87.03	[32]
Chitosan	250.63	[32]
LDH	210.00	[33]
Chitosan/Zeolite Composite	153.00	[34]
Fe-modified biochar derived from rice straw	37.00	[35]
Raw bentonite	308	This study

Table 5: ANOVA for MO adsorption by the bentonite

Source	Sum of Squares	df	Mean Square	F-value	p-value	
Model	2.424E+05	14	17316.28	47.37	< 0.0001	significant
pH(X_1)	20.74	1	20.74	0.0567	0.8146	
Time (X_2)	745.74	1	745.74	2.04	0.1713	
Concentration (X_3)	41424.95	1	41424.95	113.33	< 0.0001	
Temperature (X_4)	7819.48	1	7819.48	21.39	0.0002	
$X_1 X_2$	6.75	1	6.75	0.0185	0.8935	
$X_1 X_3$	57.66	1	57.66	0.1578	0.6962	
$X_1 X_4$	26.57	1	26.57	0.0727	0.7907	
$X_2 X_3$	2697.59	1	2697.59	7.38	0.0147	
$X_2 X_4$	149.79	1	149.79	0.4098	0.5306	
$X_3 X_4$	11790.96	1	11790.96	32.26	< 0.0001	
X_1^2	26.19	1	26.19	0.0716	0.7922	
X_2^2	798.49	1	798.49	2.18	0.1577	
X_3^2	60.80	1	60.80	0.1663	0.6885	
X_4^2	1444.81	1	1444.81	3.95	0.0631	
Residual	6213.76	17	365.52			
Lack of Fit	6213.76	7	887.68			
Pure Error	0.0000	10	0.0000			
Cor Total	2.486E+05	31				

Optimization

RSM

The coefficient of determination or fit is a test applied in the analysis of variance for identifying the best model. The researchers use R^2 -adj to measure their model precision. The R^2 -adj fit coefficient is the adjusted coefficient of determination (R^2) which is not always enhanced by increasing the factors to models. It decreases if unnecessary factors are added to the model. Statistically, a model is appropriate if it has the highest fit. It should be mentioned that this is a necessary condition [36].

The linear interactions, quadratic, two-factor (2FI), and cubic models were used in the RSM optimization of MO adsorption. The appropriate model for the adsorption process was selected based on the correlation coefficient (R^2) and low standard deviation. CCD cannot support a complete cubic model due to insufficient experimental series, so the cubic model was not recommended. In addition, the linear model is suggested but it has a mean square value of 49009.25. The quadratic model is the most useful model to characterize the adsorption of MO dye with a correlation coefficient (R^2) of 0.975. In addition, the adjusted R^2 for

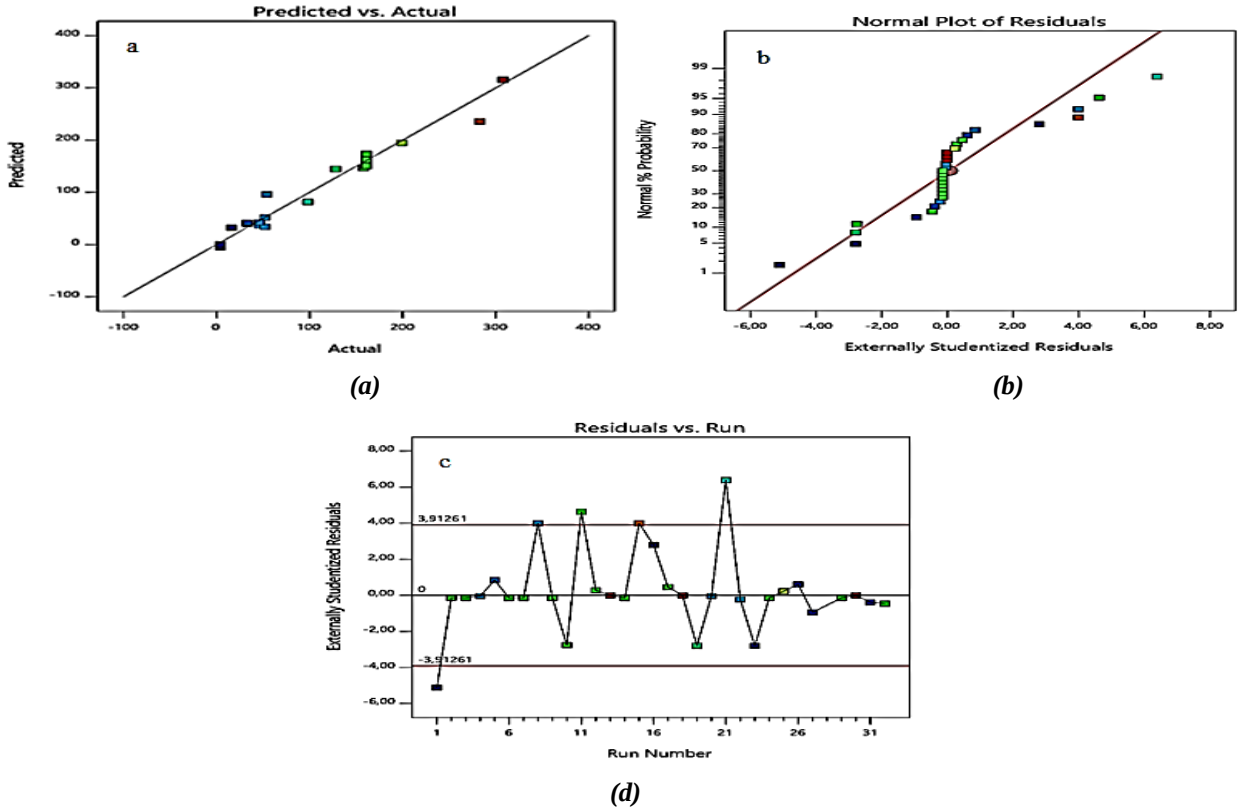

Fig. 6:. a: Evolution of predicted and actual response, b: Normal probability plot of the residual c: Residual versus run number, using the RSM model

the quadratic model was 0.9544. This value indicates high implications and an appropriate correlation between input and output values [37]. The analysis of variance (ANOVA) (Table 5) shows that the data set is significant with model F-values and p-values less than 0.0001. According to low p-values, it is possible to predict the adsorption capacity of the material using the quadratic model. These values are significant for tracking the design domain. The model of minimization was used to reduce some noisy terms that were not important and to improve the performance of the model. Pourabadeh et al. [5] obtained a high F-value and a very small P-value for Direct Red-31 and Direct Brown-2 removal models. R2 should be between zero and one if it is closer to one, it will be better, indicating high accuracy and low error in the experiments.

The results of the RSM model suggest a strong correlation between the actual and designed values of the response. Substantial association and appropriate estimation between the actual and predicted variables were observed in the model [38], which also showed adequate accuracy. In addition, the error committed is very small for the model, and the residual error is too small (Fig. 6). *Yang et al.* [39] have the same evolution in the extraction of malachite green and rhodamine B. In the ANOVA, the sum of squares for each component of the model was calculated as shown in Table 5.

Based on the sum of squares obtained from the ANOVA, the percentage of contributions (PC) for each term was identified [40]. Fig. 7 shows that the initial concentration (X_3) has the largest percentage contribution with 61.76% compared to the other components. Meng et al. [41] indicate that the ANOVA gives also the total PC values for the possible first-order, quadratic, and interaction terms according to the equations:

$$TPC_i = \frac{\sum_{i=1}^{n} SS_i}{\sum_{i=1}^{n}\sum_{i=1}^{n} SS_i + SS_{ii} + SS_{ij}} \times 100 \quad (23)$$

$$TPC_{ii} = \frac{\sum_{i=1}^{n} SS_{ii}}{\sum_{i=1}^{n}\sum_{j=1}^{n} SS_i + SS_{ii} + SS_{ij}} \times 100 \quad (24)$$

$$TPC_{ij} = \frac{\sum_{i=1}^{n}\sum_{i=1}^{n} SS_{ij}}{\sum_{i=1}^{n}\sum_{j=1}^{n} SS_i + SS_{ii} + SS_{ij}} \times 100 \quad (25)$$

Table 6: Values of R^2 and RMSE of statistical physic models

Model	Monolayer adsorption	Monolayer adsorption with two energies	Double layer adsorption	Multilayer adsorption
R^2	0.673	0.9845	0.9260	0.673
RMSE	104.8	9.47	58.97	138.7

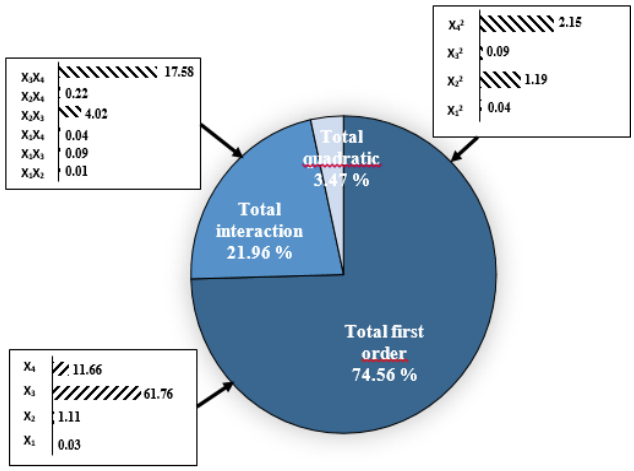

Fig. 7: Percentage of effects contribution in response formation

A detailed diagram (Fig. 7) shows the percentage contributions of the components. The TPCi of the first-order terms with the highest level of significance with a total contribution of 74.56% compared to the other TPC values. The TPCii of the interaction terms with a total contribution of 21.96%. Among the calculated TPC values, the TPCij of the quadratic terms has the lowest significance level, with a total contribution of 3.47%. These results denote that the quadratic components did not show a significant effect in predicting MO removal efficiency. So, the TPC values also prove that the first-order independent variables have a direct relationship with MO removal. The use of two-dimensional (2D) and three-dimensional (3D) plots will allow for a more effective analysis of the relationship between factors and the responses being researched. Fig. 8 and 9 shows the response surface plots derived from the polynomial model for the variation of the amount adsorbed with initial concentration, pH solution, contact time, and temperature. The actual experimental model showed that the removal efficiency of MO dye by raw bentonite is positively affected by pH, contact time, initial concentration, and temperature. The graphs also show that as opposed to pH the time contact, concentration, and temperature have a significant impact on the adsorbed quantity. *Siroos Shojaei et al.* [42] observed that with increasing sonication time, the amount of dye removal should increase. This is because, with increasing time, there is more opportunity for the dye and adsorbent molecules to be exposed. The effect of various factors (dyes concentration, sonication time, ionic strength, adsorbent dosage, temperature, and pH of the solution) on the amount of removal of malachite green and auramine-O by NaX nanozeolites removal was evaluated by the Taguchi method [43].

ANN analysis

The ANN method performs the same data used by the RSM. The target variable was the amount of MO adsorbed. The data as input variables are pH, contact time, initial concentration, and temperature. The ANN architecture used to run the algorithm model is 24 datasets (80 %), for training, while 3 datasets (10 %) are for validating and testing the model. The training algorithm is determined by the Levenberg-Marquardt method. Fig. 10 shows the evolution of the Root Mean Square Error (RMSE). We observe the decrease of the RMSE value with the rise of the training process and the number of hidden neurons. The error value reaches 10^{-26} after four epochs and there was no change in the RMSE values. Six iterations and six epochs are enough to achieve the best training performance. Fig. 11 shows the details of the training and performance. The same evolution was observed to remove hexavalent chromium by macroalgal spent biomass [44].

STATISTICAL PHYSIC THEORY

Theoretical physics statistic is a method developed to determine the adsorption mechanism. Four models of theoretical physical statistics were used in this study. Table 6 groups the values of R^2 and the RMSE error of the ensemble of the models. We remark that the monolayer model with two energies is the best suitable compared to the other models. The values of the R^2 are equal to 0.9845, and RMSE= 9.47. *M. Mobarak et al.* [45] have the same model in the case of MO adsorption by MCM–48 silica.

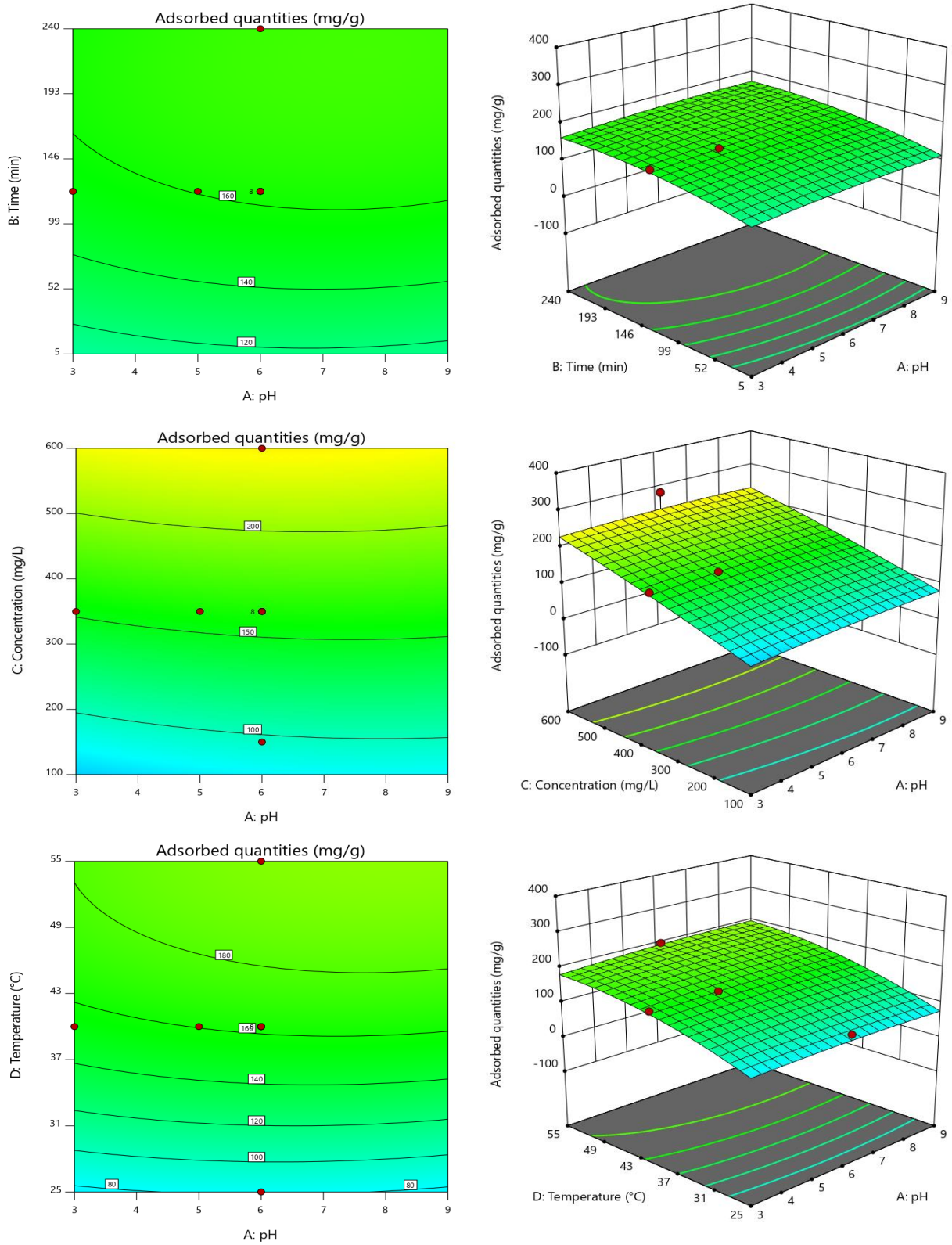

Fig. 8. 2D and 3D plot influence of pH, parameter according to RSM method

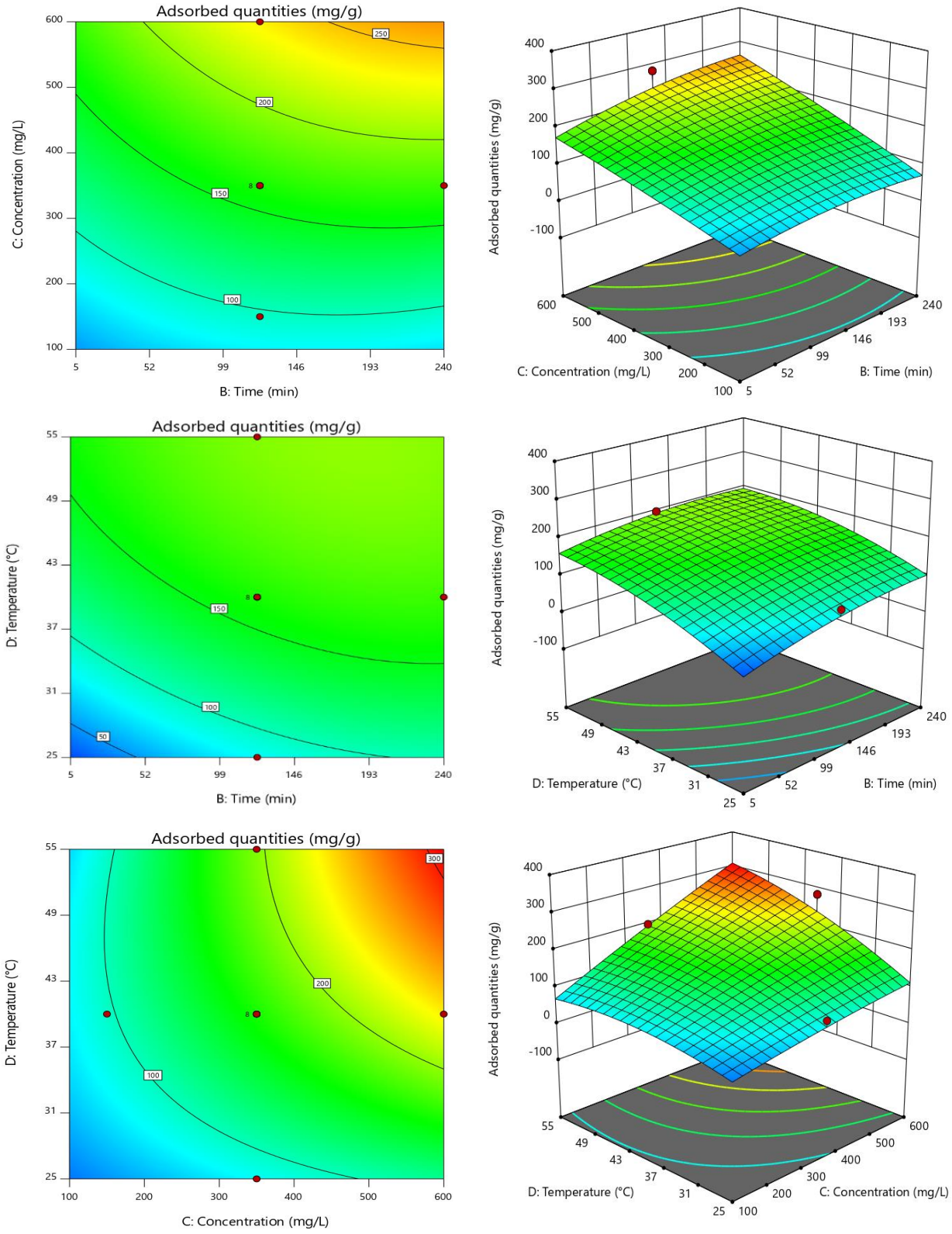

Fig. 9: 2D and 3D plot influence of time, temperature, and concentration parameters according to the RSM method

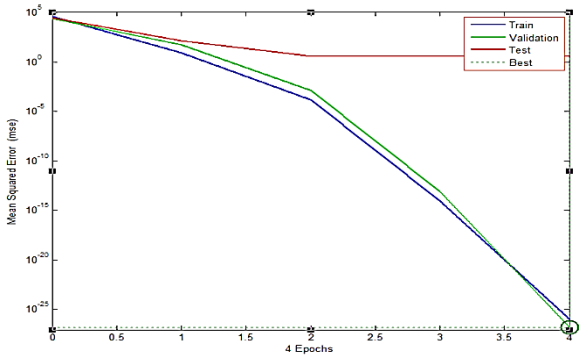

Fig. 10: ANN performance validation plot

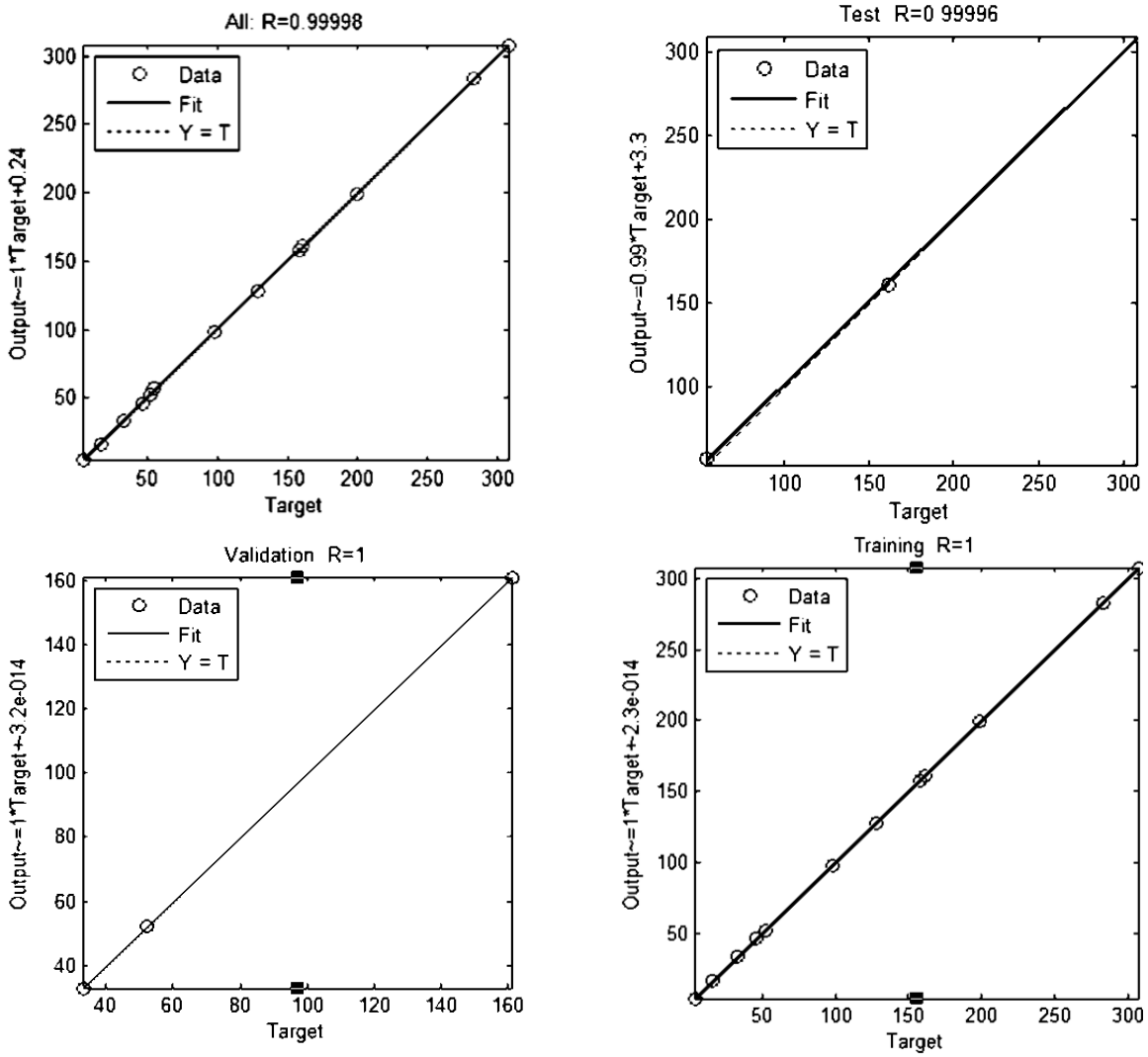

Fig. 11: Plots of predicted values versus observed values for ANN-derived models for MO adsorption

Table 7 gives the parameters of the monolayer model with two energies. We remark that whatever the temperature values of the coefficient of determination (R^2) are higher or equal to 0.98. At 25 °C, the parameters remain unchanged i.e. $n_1=n_2=1.95$, $D_{1m}=D_{2m}=57.049$ mg/g, and $C_1=C_2=295.3$ mg/L. At 40 and 55 °C, the number of MO molecules adsorbed

Table 7: Adjustment parameters value corresponding to the best fitting model

T(°C)	n_1	n_2	D_{1m} (mg/g)	D_{2m} (mg/g)	C_1 (mg/L)	C_2 (mg/L)	Q_{sat1} (mg/g)	Q_{sat2}(mg/g)	$Q_{satTotal}$(mg/g)	R^2
25	1.95	1.95	57.05	57.05	295.30	295.28	111.25	111.25	222.50	0.9845
40	18.38	2.54	2.29	116.12	249.83	172.55	42.09	294.94	337.03	0.9969
55	32.13	1.42	1.99	245.43	150.21	166.31	63.94	348.51	412.45	0.9961

Table 8: Values corresponding to the adsorption energies of the four adsorption sites in raw bentonite

Temperature (°C)	C_1 (mg/L)	C_2 (mg/L)	ΔE_{ads1} (kJ/mol)	ΔE_{ads2} (kJ/mol)
25	295.30	295.28	7.01	7.01
40	249.83	172.55	7.42	7.34
55	150.21	166.31	8.68	8.43

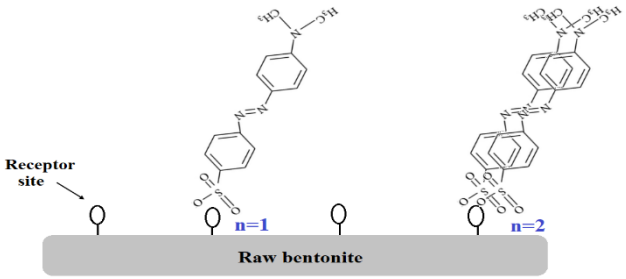

Fig. 12: Anchorage scheme for the MO dye on the raw bentonite (n_1=n_2=1.95)

per site n_2 is lower compared to n_1. All the values of n are greater than 1, indicating the agglomeration of the receptor sites. The values of n denote that the interaction of the material with the dye molecules is of non-parallel orientation. As an example, the value of n_1 and n_2 equal 1.95. These values are between 1 and 2. Indeed, the receptor site interacts with a dye molecule or two dye molecules with two respective percentages x and (1-x). The equation of this example is:

$$1.95 = 1 \times x + (1 - x) \times 2 \qquad (26)$$

The results indicate that only 5% of the receptor sites interact with one molecule, and 95% of the receptor sites gave double interactions with two dye molecules (Fig. 7). In contrast, the density of receptor sites occupied by MO for the second type is superior to the density of receptor sites occupied by MO for the first type. In addition, the adsorption capacity at saturation decreases with temperature for the first active site and increases with temperature for the second active site. The total adsorption capacity at saturation ($q_{atTotal}$) (Table 7) increases with temperature which is in agreement with the adsorption isotherms.

The interactions between the MO molecules and the material surface is determined from the adsorption energy through the
parameter C_1 and C_2 given in equation 27.

Adsorption energy (ΔE)

$$\Delta E = RTln\left(\frac{C_s}{C_{1/2}}\right) \qquad (27)$$

C_s is the solubility of tested adsorbates

Table 8 represents the values of the adsorption energy E_1 and E_2. We notice that the values of the energy E_1 and E_2 are positive and less than 40 Kj/mol, indicating that the adsorption process is physical [46,47]. *F. Dhaouadi et al.* [48] have the same evolution in the case of the removal of Pb^{2+}, $Cd^{2+,}$ and Ni^{2+} on chicken feathers.

The adsorption energy values are in agreement with the evolution of the adsorption capacity as a function of temperature. This indicates that the adsorption process of MO on the surface of raw bentonite is endothermic.

CONCLUSIONS

The XRD and SEM analysis characterize the raw bentonite with the basal spacing value (d_{001}) of 11.77 Å. The results show that silica and aluminum are the major components of the material. The adsorption of MO indicates that a pH=3 presents the best-adsorbed quantity. Equilibrium is reached after 2 hours of contact. The kinetic study indicates that the pseudo-second-order is an adequate model with R^2 ≥0.99. The amount adsorbed increases with temperature. It is 159 and 308 mg/g at 25 and 55 °C, respectively. The adsorption isotherms are best described by Langmuir-Freundlich, and Baudu models. The results of RSM and ANN suggested that the initial concentration

is the dominant parameter with a percentage contribution of 61.76% compared to the other components. The quadratic model is the most useful model to characterize the adsorption of MO dye with a correlation coefficient (R^2) of 0.975, and an adjusted R^2 of 0.9544. Physical statistical analysis reveals that the monolayer model with two energy is more appropriate. The values of adsorption energy are between 7 and 8 kJ/mol indicating that the process is physical and favored by the increase in temperature. These results prove that the material can be used for environmental remediation.

Acknowledgments

The Algerian authors wish to thank the Directorate-General of Scientific Research and Technological Development (DGRSDT, MESRS, Algeria) for its financial support.

Received : Dec. 21, 2022 ; Accepted : Apr.23, 2023

REFERENCES

[1] Shojaei S., Shojaei S., Pirkamali M., Application of Box–Behnken Design Approach for Removal of Acid Black 26 from Aqueous Solution Using Zeolite: Modeling, Optimization, and Study of Interactive Variables, *Water Conserv. Sci. Eng.*, **4(1)**: 13–19 (2019).

[2] Bessaha F., Marouf-Khelifa K., Batonneau-Gener I., Khelifa A., Characterization and Application of Heat-Treated and Acid-Leached Halloysites in the Removal of Malachite Green: Adsorption, Desorption, and Regeneration Studies, *Desalin. Water Treat.*, **57(31)**: 14609–14621 (2016).

[3] Mohamed H.S., Soliman N.K., Moustafa A.F., Abdel-Gawad O.F., Taha R.R., Ahmed S.A., Nano Metal Oxide Impregnated Chitosan-4-Nitroacetophenone for Industrial dye Removal, *Int. J. Environ. Anal. Chem.*, **101(13)**: 1850–1877 (2021).

[4] Bessaha F., Mahrez N., Marouf-Khelifa K., Çoruh A., Khelifa A., Removal of Congo red by Thermally and Chemically Modified Halloysite: Equilibrium, FTIR Spectroscopy, and Mechanism Studies, *Int. J. Environ. Sci. Technol.*, **16(8)**: 4253–4260 (2019).

[5] Pourabadeh A., Baharinikoo L., Shojaei S., Mehdizadeh B., Davoodabadi Farahani M., and Shojaei S., Experimental Design and Modelling of Removal of Dyes Using Nano-Zero-Valent Iron: A Simultaneous Model, *Int. J. Environ. Anal. Chem.*, **100(15)**: 1707–1719 (2020).

[6] Bessaha G., Bessaha F., Bendenia S., Khelifa A., Exchanged Zeolite Adsorbent for Removing Cr(VI): Kinetics, Thermodynamics and Adsorption Mechanism, *Int. J. Environ. Anal., Chem.*, 1–19 (2022).

[7] Mahrez N., Bessaha F., Marouf-Khelifa K., Çoruh A., Khelifa A., Performance and Mechanism of Interaction of Crystal Violet with Organohalloysite, *Desalin. Water Treat.*, **207**: 410–419 (2020).

[8] Rahman O., Rahman M.M., Maniruzzaman M., Removal of dye and Heavy Metals from Industrial Wastewater by Activated Charcoal-Banana Rachis Cellulose Nanocrystal Composites Filter, *Int. J. Environ. Anal. Chem.*, 1–19 (2022).

[9] Karthick Raja Namasivayam S., Pattukumar V., Samrat K., Kumar J.A., Arvind Bharani R.S., Alothman A.A., Osman S.M., Tran V.A., Rajasimman M., Evaluation of Methyl Orange Adsorption Potential of Green Synthesized Chitosan-Silver Nanocomposite (CS–AgNC) and its Notable Biocompatibility on Freshwater Tilapia (Oreochromis Nitoticus), *Chemosphere*, **308**: 135950 (2022).

[10] Aichour A., Zaghouane-Boudiaf H., Djafer Khodja H., Highly Removal of Anionic Dye from Aqueous Medium Using a Promising Biochar Derived from Date Palm Petioles: Characterization, Adsorption Properties and Reuse Studies, *Arab. J. Chem.*, **15(1)**: 103542 (2022).

[11] Msaadi R., Yahia A., Sassi W., Ammar S., Adsorption of Methyl Orange onto Perlite: Optimization, Adsorption Kinetics, and Thermodynamic Studies, *Chem. Africa*, (2022).

[12] Mirzaei D., Zabardasti A., Mansourpanah Y., Sadeghi M., Farhadi S., Efficacy of Novel NaX/MgO–TiO2 Zeolite Nanocomposite for the Adsorption of Methyl Orange (MO) Dye: Isotherm, Kinetic and Thermodynamic Studies, *J. Inorg. Organomet. Polym. Mater.*, **30(6)**: 2067–2080 (2020).

[13] Yang J., Shojaei S., Shojaei S., Removal of Rudg and dye from Aqueous Solutions by Graphene Oxide: Adsorption Studies and Chemometrics Methods, *NPJ Clean Water*, **5(1)**: 5 (2022).

[14] Belkassa K., Bessaha F., Marouf-Khelifa K., Batonneau-Gener I., Comparot J., Khelifa A., Physicochemical and Adsorptive Properties of a Heat-Treated and Acid-Leached Algerian Halloysite, *Colloids Surfaces, A Physicochem. Eng. Asp.*, **421**: 26–33 (2013).

[15] Salaa F., Bendenia S., Lecomte-Nana G.L., Khelifa A., Enhanced Removal of Diclofenac by an Organohalloysite Intercalated Via a Novel Route: Performance and Mechanism, *Chem. Eng. J.*, 396(18):125226 (2020).

[16] Shojaei S., Shojaei S., Optimization of Process Variables by the Application of Response Surface Methodology for Dye Removal Using Nanoscale Zero-Valent Iron, *Int. J. Environ. Sci. Technol.*, **16(8)**: 4601–4610 (2019).

[17] Fernandes C.D., Nascimento V.R.S., Meneses D.B., Vilar D.S., Torres N.H., Leite M.S., Vega Baudrit J.R., Bilal M., Iqbal H.M.N., Bharagava R.N., Egues S.M., Romanholo Ferreira L.F., Fungal Biosynthesis of Lignin-Modifying Enzymes From Pulp Wash and Luffa Cylindrica for Azo Dye RB5 Biodecolorization Using Modeling by Response Surface Methodology and Artificial Neural Network, *J. Hazard. Mater.*, 399 (2020).

[18] Anbazhagan S., Thiruvengatam V., Kulanthai K., Adaptive Neuro-Fuzzy Inference System and Artificial Neural Network Modeling for the Adsorption of Methylene Blue by Novel Adsorbent in a Fixed - Bed Column Method, *Iran. J. Chem. Chem. Eng. (IJCCE)*, **39(6)**: 75–93 (2020).

[19] Kamari E., Hajizadeh A.A., Kamali M.R., Experimental Investigation and Estimation of Light Hydrocarbons Gas-Liquid Equilibrium Ratio in Gas Condensate Reservoirs through Artificial Neural Networks, *Iran. J. Chem. Chem. Eng. (IJCCE)*, **39(6)**: 163–172 (2020).

[20] Hafeez A., Ammar Taqvi S.A., Fazal T., Javed F., Khan Z., Amjad U.S., Bokhari A., Shehzad N., Rashid N., Rehman S., Rehman F., Optimization on Cleaner Intensification of Ozone Production Using Artificial Neural Network and Response Surface Methodology: Parametric and Comparative Study, *J. Clean. Prod.*, **252**: 119833 (2020).

[21] Zhirong L., Azhar Uddin M., Zhanxue S., FT-IR and XRD analysis of natural Na-bentonite and Cu(II)-loaded Na-Bentonite, *Spectrochim. Acta - Part A Mol. Biomol. Spectrosc.*, **79(5)**: 1013–1016 (2011).

[22] Kıpçak İ. Kalpazan E., Preparation of CoB Catalysts Supported on Raw and Na-Exchanged Bentonite Clays and Their Application in Hydrogen Generation from the Hydrolysis of NaBH4, *Int. J. Hydrogen Energy*, **45(50)**: 26434–26444 (2020).

[23] Pan J., Zhou L., Chen H., Liu X., Hong C., Chen D., Pan B., Mechanistically Understanding Adsorption of Methyl Orange, Indigo Carmine, and Methylene Blue onto Ionic/Nonionic Polystyrene Adsorbents., *J. Hazard. Mater.*, **418**: 126300 (2021).

[24] Ba Mohammed B., Lgaz H., Alrashdi A.A., Yamni K., Tijani N., Dehmani Y., Hamdani H. El, Chung I.-M., Insights into Methyl Orange Adsorption Behavior on a Cadmium Zeolitic-Imidazolate Framework Cd-ZIF-8: A joint Experimental and Theoretical Study," *Arab. J. Chem.*, **14(1)**: 102897 (2021).

[25] Alhalili Z., Green Synthesis of Copper Oxide Nanoparticles CuO NPs from Eucalyptus Globoulus leaf Extract: Adsorption and Design of Experiments, *Arab. J. Chem.*, **15(5)**: 103739 (2022).

[26] Giles C., H., DAVID S., A General Treatment and Classification of the Solute Adsorption Isotherm I. Theoretical, *J. Colloid Interface Sci.*, **47**: 755–765 (1974).

[27] Jasrotia R., Singh J., Mittal S., Singh H.S., Synthesis of CTAB Modified Ferrite Composite for the Efficient Removal of Brilliant Green Dye, *Int. J. Environ. Anal. Chem.*, (2022).

[28] Onu C.E., Nwabanne J.T., Ohale P.E., Asadu C.O., Comparative Analysis of RSM, ANN and ANFIS and the Mechanistic Modeling in Eriochrome black-T dye Adsorption Using Modified Clay, *South African J. Chem. Eng.*, **36**: 24–42 (2021).

[29] Hosseini S., Khan M.A., Malekbala M.R., Cheah W., Choong, T.S.Y., Carbon Coated Monolith, A Mesoporous Material for the Removal of Methyl Orange from Aqueous Phase: Adsorption and Desorption Studies, *Chem. Eng. J.*, **171**: 1124–1131 (2011).

[30] Cheah W., Hosseini S., Khan M.A., Chuah T.G., Choong T.S.Y., Acid Modified Carbon Coated Monolith for Methyl Orange Adsorption, *Chem. Eng. J.*, **215–216**: 747–754 (2013).

[31] Li Y., Suia K., Liub R., Zhaoa X., Zhanga Y., Lianga H., Xia Y., Energy Procedia Removal of Methyl Orange from Aqueous Solution by Calcium Alginate / Multi-walled Carbon Nanotubes Composite Fibers, *Int. Conf. Futur. Energy, Environ. Mater. Remov.*, **16**: 863–868 (2012).

[32] Chen H., Zhao J., Wu J., Dai G., Isotherm, Thermodynamic, Kinetics and Adsorption Mechanism Studies of Methyl Orange by Surfactant Modified Silkworm Exuviae, *J. Hazard. Mater.*, **192**: 246–254 (2011).

[33] Zaghloul A., Benhiti R., Ait Ichou A., Carja G., Soudani A., Zerbet M., Sinan F., Chiban M., Characterization and Application of MgAl Layered Double Hydroxide for Methyl Orange Removal from Aqueous Solution, *Mater. Today Proc.*, **37**: 3793–3797 (2020).

[34] Habiba U., Siddique T.A., Jia J., Lee L., Joo T.C., Ang B.C., Afifi A.M., Adsorption Study of Methyl Orange by Chitosan/Polyvinyl Alcohol/Zeolite Electrospun Composite Nanofibrous Membrane, *Carbohydr. Polym.*, 1–20 (2018).

[35] Nguyen L.X., Do, P.M.T., Phan T.T.T., Nguyen C.H., Downes N.K., Removal of Anions P_3O_4- and Methyl Orange Using Fe-Modified Biochar Derived from Rice Straw, *Iran. J. Chem. Chem. Eng. (IJCCE)*, **42(3)**: 821–834 (2023).

[36] Shojaei S., Nouri A., Baharinikoo L., Davoodabadi Farahani M., Shojaei S., Removal of the Hazardous Dyes through Adsorption Over Nanozeolite-X: Simultaneous Model, Design and Analysis of Experiments, *Polyhedron*, **196**: 114995 (2021).

[37] Vainio A., Pulkka A., Paloniemi R., Varho V., Tapio P., Citizens' Sustainable, Future-Oriented Energy Behaviours in Energy Transition, *J. Clean. Prod.*, **245(xxxx)**: 118801 (2020).

[38] Pedram T., Esamp haghi Z., Ahmadpour A., Nakhaei A., Optimization of Adsorption Parameters Using Central Composite Design for the Removal of Organosulfur in Diesel Fuel by Bentonite-Supported Nanoscale NiO-WO_3, *Iran. J. Chem. Chem. Eng. (IJCCE)*, **41(3)**: 808–820 (2022).

[39] Yang J. Shojaei S., Removal of Drug and Dye from Aqueous Solutions by Graphene Oxide : Adsorption Studies and Chemometrics Methods, *NPJ. Clean Water*, **5(5)**: 1–10 (2022).

[40] Bakhtiari G., Bazmi M., Abdouss M., Royaee S.J., Adsorption and Desorption of Sulfur Compounds by Improved Nano Adsorbent: Optimization Using Response Surface Methodology, *Iran. J. Chem. Chem. Eng. (IJCCE)*, **36(4)**: 69–79 (2017).

[41] Meng H. Neville A., A Systematic Erosion–Corrosion Study of two Stainless Steels in Marine Conditions via Experimental Design, *Wear*, **263**: 355–362 (2007).

[42] Shojaei S., Shojaei S., Nouri A., Baharinikoo L., Application of Chemometrics for Modeling and Optimization of Ultrasound-Assisted Dispersive Liquid – Liquid Microextraction for the Simultaneous Determination of Dyes, *NPJ Clean Water*, 1–8 (2021).

[43] Shojaei S., Shojaei S., Band S.S., Abbas A., Farizhandi K., Application of Taguchi Method and Response Surface Methodology into the Removal of Malachite Green and Auramine - O by NaX Nanozeolites, *Sci. Rep.*, 1–13 (2021).

[44] Vinayagam R., Dave N., Varadavenkatesan T., Rajamohan N., Sillanpää M., Nadda A.K., Govarthanan M., Selvaraj R., Artificial Neural Network and Statistical Modelling of Biosorptive Removal of Hexavalent Chromium Using Macroalgal Spent Biomass, *Chemosphere*, **296**: 133965 (2022).

[45] Mobarak M., Mohamed E.A., Selim A.Q., Mohamed F.M., Sellaoui L., Bonilla-Petriciolet A., Seliem M.K., Statistical Physics Modeling and Interpretation of Methyl Orange Adsorption on High–Order Mesoporous Composite of MCM–48 Silica with Treated Rice Husk, *J. Mol. Liq.*, **285**: 678–687 (2019).

[46] Ward T.M. Upchurch R.P., Herbicide Adsorption, Role of Amido Group in Adsorption Mechanisms, *J. Agric. Food Chem.*, **13**: 334–340 (1965).

[47] Oepen B. von Kördel W., Klein W., Sorption of Nonpolar and Polar Compounds to Soils: Processes, Measurements and Experience with the Applicability of the Modified OECD-Guideline 106, *Chemosphere*, **22(3)**: 285–304 (1991).

[48] Dhaouadi F., Sellaoui L., Badawi M., Reynel-Ávila H.E., Mendoza-Castillo D.I., Jaime-Leal J.E., Bonilla-Petriciolet A., Lamine A. B., Statistical Physics Interpretation of the Adsorption Mechanism of Pb2+, Cd^{2+} and Ni^{2+} on Chicken Feathers, *J. Mol. Liq.*, **319**: 114168 (2020).